Nanoscale

Accepted Manuscript

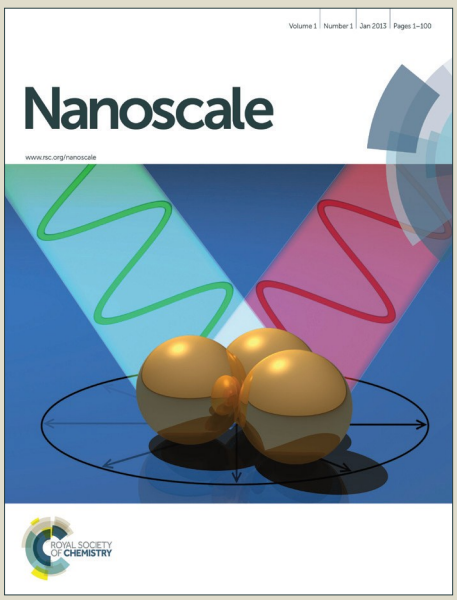

ROYAL SOCIETY OF CHEMISTRY

www.rsc.org/nanoscale

Nanoscale

RSCPublishing

COMMUNICATION

An effective strategy of magnetic stem cell delivery for spinal cord injury therapy†

Cite this: DOI: 10.1039/x0xx00000x

Dmitry Tukmachev,[ab] Oleg Lunov,[*c] Vitalii Zablotskii,[c] Alexandr Dejneka,[c] Michal Babic,[d] Eva Syková,[ab] Šárka Kubinová,[*ab]

Received 00th January 2014,
Accepted 00th January 2014

DOI: 10.1039/x0xx00000x

www.rsc.org/

Spinal cord injury (SCI) is a condition that results in significant mortality and morbidity. Treatment of SCI utilizing stem cell transplantation represents a promising therapy. However, current conventional treatments are limited by inefficient delivery strategies of cells into the injured tissue. In this study, we designed a magnetic system and used it to accumulate stem cells labelled with superparamagnetic iron oxide nanoparticles (SPION) at a specific site of a SCI lesion. The loading of stem cells with engineered SPIONs that guarantees sufficient attractive magnetic forces was achieved. Further, the magnetic system allowed rapid guidance of the SPION-labelled cells precisely to the lesion location. Histological analysis of cell distribution throughout the cerebrospinal channel showed a good correlation with the calculated distribution of magnetic forces exerted onto the transplanted cells. The results suggest that focused targeting and fast delivery of stem cells can be achieved using the proposed non-invasive magnetic system. With future implementation the proposed targeting and delivery strategy bears advantages for the treatment of disease requiring fast stem cell transplantation.

Spinal cord injury (SCI) represents a devastating condition that leads to a dramatic disability, loss of voluntary movement, tactile sensibility, and is accompanied by chronic pain and spasticity.[1, 2] Currently there is no available restorative therapy for SCI, only prevention is identified as the best medicine.[2, 3] The transplantation of stem cells, particularly mesenchymal stem cells (MSCs), holds considerable potential as effective SCI therapies.[2-4] Despite the noticed therapeutic benefits, stem cell transplantation, in general, has a number of serious limitations related to the low efficiency of delivery, retention and engraftment of cells.[5, 6] To achieve a significant therapeutic benefit, minimally invasive but highly effective delivery strategies are a crucial aspect of cell transplantation. Interestingly, intrathecal injection of stem cells has considerable advantages (higher efficacy of delivery, better retention and survival of stem cells) over intravenous injection as a means of cell transplantation.[7-9] Moreover, it has been demonstrated that repetitive, but not single intrathecal administration of MSCs contributes to their migration into the central lesion and aids functional recovery after SCI in rats.[10] Effective cell targeting is therefore highly desirable in order to promote the homing of transplanted cells to the site of injury. In this regard, the use of magnetic nanomaterials represents novel effective treatment, particularly in SCI.[11] Several research lines have demonstrated the efficient loading of stem cells with superparamagnetic iron oxide nanoparticles (SPIONs) and have shown that magnetically guided cell delivery is able to boost cell retention, engraftment as well as the functional benefit of the cell therapy.[12-14] Indeed, magnetic forces have already been successfully used in directing SPION-labelled cells to a vascular graft[15], intra-arterial stents[16], the femoral artery[17], bone[18], cartilage[19], and the retina.[20] However, in the case of SCI, studies on magnetically guided cell delivery have not been thoroughly performed. In fact, only two research groups have shown the therapeutic potential of the magnetic delivery of SPION-labelled cells to the SCI lesion site.[21-23] A common disadvantage of all the previous strategies of cell delivery that utilize magnetic systems[16, 17, 24, 25] is their inappropriate focusing ability. Indeed, magnetic cell capturing takes place in the vicinity of a magnetic pole where the magnetic field gradient is at its maximal value. Since a magnet cannot be placed directly into the lesion site, the focusing ability of such systems is rather limited and not convenient for efficient stem cell transplantation.

Here we propose a new magnetic system consisting of two cylindrical NdFeB magnets (1 cm diameter and 5 cm height, out-of-plane remanent magnetization values 1.2 T) placed on a ring-shaped holder with the alike poles facing toward each other. A specific feature of the proposed magnetic system is the existence of a focusing zone – *trapping area* – where both the horizontal and

vertical magnetic force components (*X*- and *Z*- components) are almost zero (Fig. 1 and 2). This focusing zone is located just between the two maxima of the planar components (parallel to the *X*-*Z*-axis) of the magnetic gradient force (Fig. 2A, B and C). Thus, the magnetically labelled cells have to be focused namely in this trapping area. The existence of the trapping area (with zero magnetic forces) is determined by two reasons: i) the maximums of the planar and vertical components of the magnetic field (MF) gradient must reach close to the magnets' edges; ii) in the mirror symmetry plane of the system the planar and vertical components of the MF gradients have opposite directions and compensate for each other. Figure 2 shows the magnetic force distributions in the *X*-*Z*-plane between two magnets with opposing magnetisations that were calculated analytically using the explicit expressions for the magnetic stray fields produced by a uniformly magnetized magnet.[25] The area outlined by the ellipse represents the focusing zone for the given configuration of the magnetic poles and their geometry. In this study we exploit this magnetic system to enhance the efficacy of stem cell delivery using rat models of SCI. The experiments were carried out in following groups of animals: SPION-labelled MSCs exposed to MF, non-labelled MSCs exposed to MF and SPION-labelled MSCs without exposure to MF. One week after the induction of the lesion, 5 x 10^5 cells were injected intrathecally at the *L5*-*L6* level, at a distance of 10 cm from the lesion site (Fig. 1A and B). Subsequently, the above-described external magnetic system was placed around the rat, under the top of the vertebral column above the lesion site at *Th10*, for two hours to improve cell retention and attachment (Fig. 1A and B). For MSCs labelling the poly-*L*-lysine-coated SPIONs were chosen as non-toxic and non-inducing pathophysiological effects nanoparticles as described in our previously performed biocompatibility screening.[26-28]

First, we tested whether the MSCs labelled with SPIONs (Fig. 2D) can be efficiently attracted by a magnet *in vitro* (Fig. 3A). Second, *in vivo* experiments (which scheme is depicted in Fig.1) showed dramatic increase of SPION-labelled cell retention at the lesion site (Fig. 3B and 4B, C). On the other hand, cells without ~~SIPONs~~ SPIONs and cells loaded with SPIONs but with no magnets exhibited practically homogenous distribution through the spinal cord channel (Fig.3B). ~~The latter implies that molecular cues generated by the lesion site are not able to assist the cell retention.~~ This means that the lesion itself, which releases various chemoattractans, is not able to retain the transplanted cells and therefore enhance their homing to the damaged tissue area. It is worth noting that the cell distribution in the vicinity of the lesion site (Fig. 3B) was quantitatively consistent with the calculated magnetic gradient force distribution (Fig. 2B and C): SPION-labelled cells accumulated maximally in the trapping area of the magnetic system (Fig. 3B and 4A). Moreover, the number of SPION-labelled cells in the centre of the lesion was significantly higher when compared to the control groups (Fig. 3). Furthermore, very few cells were detected in the cranial direction from the magnetic gradient force (Fig. 3B and 4A), which verifies the capture of the SPION-labelled cells within the MF. In contrast, non-labelled cells used with MF and SPION-labelled cells without MF revealed a homogeneous distribution without any apparent effect of the MF on cell accumulation at SCI lesion site (Fig. 3B). Aside from this, the use of the magnetic system resulted in a significant increase in SPION-labelled cell accumulation directly in the lesion site in comparison to no MF application (Fig. 4B and C). The ratio (*E*) between the number of cells captured in the lesion site and the total number of cells in the operating range of the spinal cord may serve as a convenient measure of the efficiency of cell delivery. From Fig. 3B the ratio *E* was calculated for three studied animal groups: *E* = 45 % for the SPION-labelled MSCs exposed to MF; *E* = 14 % for the non-labelled MSCs exposed to MF and *E* = 13 % for the SPION-labelled MSCs without exposure to MF. Thus, there is an obvious advantage of the proposed magnetic delivery strategy resulting in a 3-fold increase of the ratio *E*. Furthermore, migration of stem cells from the cerebrospinal fluid into tissue has been associated with a better prognosis of SCI treatment.[29] Interestingly, the application of MF for 2 h resulted in stem cell infiltration into the tissue (Fig. 4B and C). Finally, the designed magnetic system targeted SPION-labelled cells to the trapping area (Fig. 4D), as revealed by superimposing the immunofluorescence images with the calculated normalized magnetic force distribution (Fig. 4D). However, after stem cell delivery to the lesion site, an adverse reaction occurred. Microglia/macrophages attacked the SPION-labelled stem cells (Fig. 4E). Thus, the long-term effects of transplanted SPION-labelled stem cells should be investigated in more detail in future studies. Consequently, because of the obvious advantages of the stem cell-based SCI therapy, we should look further for a pharmacological (or any other) strategy to counteract the impact of SPION-derived adverse effects *in vivo*. In future studies, the efficacy of such a magnetic targeting strategy and the possibilities of reaching therapeutic concentrations should be assessed together with the physiological and biological factors that decrease the number of captured living cells at the lesion site.

Conclusions

A minimally invasive magnetic targeting strategy enabling fast cell retention after intrathecal transplantation was designed and tested *in vivo*. Its main advantage is the ability to reach a significantly higher concentration of SPION-labelled stem cells into the vicinity of a lesion site. We succeeded in efficiently delivering stem cells to lesions within the animal anaesthesia time period, 2 hours. In our experiments, in contrast to the control non-magnetic groups, the SPION-labelled cells were able to migrate from the trapping area to the lesion site (Fig. 4C). It is worth noting that the efficacy of stem cell transplantation to the lesion site is low and variable,[30] with typical delivery time to SCI varying from 12 to 24 h.[22, 31, 32] Therefore, the application of our magnetic system for targeted stem cell delivery into SCI lesions demonstrates the potential benefits of fast and efficient cell delivery. The proposed strategy can be used for stem cell-based treatments of not only traumatic SCIs, but also for non-traumatic SCI or neurodegenerative diseases.[33, 34] The fate and regenerative capacity of magnetically labelled MSCs after their forced accumulation near the lesion would be a challenging direction for further study.

Acknowledgements

This work was supported by grants GACR ~~P304/11/0731~~, P304/12/1370, grant of Academy of Sciences of the Czech Republic M100101219, the Fellowship J.E. Purkyne (ASCR) and MEYS CR EE2.3.30.0029 and NPU I: LO1309. Authors thank Thomas Simmet for fruitful discussions.

Notes and references

[a]Institute of Experimental Medicine, ASCR, 14200 Prague, Czech Republic. E-mail: sarka.k@biomed.cas.cz; Fax: +420-241062706; Tel: +420-241062635

[b]Department of Neuroscience, 2nd Faculty of Medicine, Charles University, 14220 Prague, Czech Republic
[c]Institute of Physics, ASCR, 18221 Prague, Czech Republic. E-mail: lunov@fzu.cz; Fax: +420-286581448; Tel: +420-266052131
[d]Institute of Macromolecular Chemistry, ASCR, 16206 Prague Czech Republic

† Electronic Supplementary Information (ESI) available: Experimental procedures. See DOI: 10.1039/c000000x/

1 E. J. Bradbury and S. B. McMahon, *Nat. Rev. Neurosci.*, 2006, **7**, 644-653.
2 S. Thuret, L. D. F. Moon and F. H. Gage, *Nat. Rev. Neurosci.*, 2006, **7**, 628-643.
3 A. Antonic, E. S. Sena, J. S. Lees, T. E. Wills, P. Skeers, P. E. Batchelor, M. R. Macleod and D. W. Howells, *PLoS Biol.*, 2013, **11**, e1001738.
4 A. P. Pego, S. Kubinova, D. Cizkova, I. Vanicky, F. M. Mar, M. M. Sousa and E. Sykova, *J. Cell. Mol. Med.*, 2012, **16**, 2564-2582.
5 I. L. Weissman, *Science*, 2000, **287**, 1442-1446.
6 A. Al Kindi, Y. Ge, D. Shum-Tim and R. C. J. Chiu, *Front. Biosci.*, 2008, **13**, 2421-2434.
7 S. Pluchino, A. Quattrini, E. Brambilla, A. Gritti, G. Salani, G. Dina, R. Galli, U. Del Carro, S. Amadio, A. Bergami, R. Furlan, G. Comi, A. L. Vescovi and G. Martino, *Nature*, 2003, **422**, 688-694.
8 S. F. Wu, Y. Suzuki, M. Kitada, K. Kataoka, M. Kitaura, H. Chou, Y. Nishimura and C. Ide, *Neurosci. Lett.*, 2002, **318**, 81-84.
9 A. Bakshi, C. Hunter, S. Swanger, A. Lepore and I. Fischer, *J. Neurosurg.-Spine*, 2004, **1**, 330-337.
10 D. Cizkova, I. Novotna, L. Slovinska, I. Vanicky, S. Jergova, J. Rosocha and J. Radonak, *J. Neurotrauma*, 2011, **28**, 1951-1961.
11 J. Y. Tyler, X. M. Xu and J. X. Cheng, *Nanoscale*, 2013, **5**, 8821-8836.
12 N. Landazuri, S. Tong, J. Suo, G. Joseph, D. Weiss, D. J. Sutcliffe, D. P. Giddens, G. Bao and W. R. Taylor, *Small*, 2013, **9**, 4017-4026.
13 A. C. Vandergriff, T. M. Hensley, E. T. Henry, D. L. Shen, S. Anthony, J. Y. Zhang and K. Cheng, *Biomaterials*, 2014, **35**, 8528-8539.
14 K. Cheng, D. Shen, M. T. Hensley, R. Middleton, B. Sun, W. Liu, G. De Couto and E. Marban, *Nat. Commun.*, 2014, **5**, 4880.
15 S. V. Pislaru, A. Harbuzariu, G. Agarwal, T. Witt, R. Gulati, N. P. Sandhu, C. Mueske, M. Kalra, R. D. Simari and G. S. Sandhu, *Circulation*, 2006, **114**, 314-318.
16 B. Polyak, I. Fishbein, M. Chorny, I. Alferiev, D. Williams, B. Yellen, G. Friedman and R. J. Levy, *Proc. Natl. Acad. Sci. U. S. A.*, 2008, **105**, 698-703.
17 J. Riegler, A. Liew, S. O. Hynes, D. Ortega, T. O'Brien, R. M. Day, T. Richards, F. Sharif, Q. A. Pankhurst and M. F. Lythgoe, *Biomaterials*, 2013, **34**, 1987-1994.
18 S. Panseri, C. Cunha, T. D'Alessandro, M. Sandri, A. Russo, G. Giavaresi, M. Marcacci, C. T. Hung and A. Tampieri, *PLoS One*, 2012, **7**, e38710.
19 G. Kamei, T. Kobayashi, S. Ohkawa, W. Kongcharoensombat, N. Adachi, K. Takazawa, H. Shibuya, M. Deie, K. Hattori, J. L. Goldberg and M. Ochi, *Am. J. Sports Med.*, 2013, **41**, 1255-1264.
20 A. Yanai, U. O. Hafeli, A. L. Metcalfe, P. Soema, L. Addo, C. Y. Gregory-Evans, K. Po, X. Shan, O. L. Moritz and K. Gregory-Evans, *Cell Transplant.*, 2012, **21**, 1137-1148.
21 K. Nishida, N. Tanaka, K. Nakanishi, N. Kamei, T. Hamasaki, S. Yanada, Y. Mochizuki and M. Ochi, *Neuroreport*, 2006, **17**, 1269-1272.
22 V. Vanecek, V. Zablotskii, S. Forostyak, J. Ruzicka, V. Herynek, M. Babic, P. Jendelova, S. Kubinova, A. Dejneka and E. Sykova, *Int. J. Nanomed.*, 2012, **7**, 3719-3730.
23 T. Hamasaki, N. Tanaka, N. Kamei, O. Ishida, S. Yanada, K. Nakanishi, K. Nishida, Y. Oishi, S. Kawamata, N. Sakai and M. Ochi, *Spine*, 2007, **32**, 2300-2309.
24 U. O. Häfeli, K. Gilmour, A. Zhou, S. Lee and M. E. Hayden, *J. Magn. Magn. Mater.*, 2006, **311**, 323-329.
25 V. Zablotskii, J. M. Pastor, S. Larumbe, J. I. Pérez-Landazábal, V. Recarte and C. Gómez-Polo, *AIP Conf. Proc.*, 2010, **1311**, 152-157.
26 B. Novotna, P. Jendelova, M. Kapcalova, P. Rossner, K. Turnovcova, Y. Bagryantseva, M. Babic, D. Horak and E. Sykova, *Toxicol. Lett.*, 2012, **210**, 53-63.
27 O. Lunov, T. Syrovets, B. Buchele, X. Jiang, C. Rocker, K. Tron, G. U. Nienhaus, P. Walther, V. Mailander, K. Landfester and T. Simmet, *Biomaterials*, 2010, **31**, 5063-5071.
28 O. Lunov, T. Syrovets, C. Rocker, K. Tron, G. U. Nienhaus, V. Rasche, V. Mailander, K. Landfester and T. Simmet, *Biomaterials*, 2010, **31**, 9015-9022.
29 E. Sykova and P. Jendelova, *Cell Death Differ.*, 2007, **14**, 1336-1342.
30 B. Neuhuber, B. T. Himes, J. S. Shumsky, G. Gallo and I. Fischer, *Brain Res.*, 2005, **1035**, 73-85.
31 L. Fan, F. Du, B. C. Cheng, H. Peng and S. Q. Liu, *Chin. J. Traumatol.*, 2008, **11**, 94-97.
32 V. Donega, C. H. Nijboer, G. van Tilborg, R. M. Dijkhuizen, A. Kavelaars and C. J. Heijnen, *Exp. Neurol.*, 2014, **261C**, 53-64.
33 E. Sykova, A. Homola, R. Mazanec, H. Lachmann, S. L. Konradova, P. Kobylka, R. Padr, J. Neuwirth, V. Komrska, V. Vavra, J. Stulik and M. Bojar, *Cell Transplant.*, 2006, **15**, 675-687.
34 S. Forostyak, P. Jendelova and E. Sykova, *Biochimie*, 2013, **95**, 2257-2270.

Figure legends

Fig. 1 Magnetic system for MSC targeting into SCI. (A) *In vivo* application of the non-invasive magnetic system for MSC targeting into SCI of a rat. (B) Schematic representation of the magnetic targeting strategy.

Fig. 2 Spatial distribution of the magnetic gradient forces between the magnets of the designed magnetic system. (A) Calculated vector field plot of the magnetic gradient force (*X*-*Z*-plane - the vertical cross-section of the spinal cord). The insert represents an enlarged region of the trapping area (zero-force zone). The arrows show the directions of the magnetic gradient forces ($f_m \propto \nabla B^2$) applied to a cell (where B is the magnetic induction). (B) Modulus of magnetic gradient force, $\left|(\vec{B}\vec{\nabla})\vec{B}\right|$, normalized to $(\mu_0 M_r)^2 r^{-1}$, as a function of the X- coordinate which is along the cerebrospinal channel (M_r represents the remanent magnetization and $\mu_0 M_r$=1.2 T for the used magnets, magnet radius r=0.5 cm). In (A) and (B) the focusing area is shown by the green ellipses. (C) 3D plot of the normalized magnetic gradient force (*X*-*Z*-plane).

Fig. 3 Distributions of SPION- labelled cells and non-labelled cells with and without the magnetic field. (A) Attraction of SPION-labelled cells to a cylindrical magnet *in vitro*. MSCs were labelled with SPIONs at a concentration of 15.4 μg mL^{-1} and exposed to an external magnetic field for 48 h. Cells were stained for intracellular iron using Prussian blue. Scale bar: 100 μm. (B) Numbers of the captured SPION-labelled cells and non-labelled cells in the rat model as a function of the distance from the lesion site of the SCI. After the induction of the lesion, SPION- labelled MSCs were injected intrathecally at the *L5*-*L6* level, at a distance of 10 cm from the lesion site. Thereafter, animals were subjected to the magnetic system exposure for 2 h in longitudinal spinal cord segments. The dotted curves represent the respective magnetic gradient force distribution taken from Fig. 2B. Data are expressed as mean ± SEM, $^*P < 0.05$.

Fig. 4 Longitudinal spinal cord sections of the targeted SPIONs-labelled MSCs. (A) Spinal cord sections of SPION-labelled MSCs captured in the trapping area of the magnetic system. Scale bar – 1 mm. (B) Longitudinal sections of the lesion site showing MSC distribution within the lesion with or without exposure to the magnetic field. The arrows show clusters of delivered SPION-labelled MSCs ~~to the lesion site~~ on the surface of the spinal cord (Region 1) and SPION labelled MSCs that migrated in the deeper area of the lesion (Region 2). Scale bar – 500 μm. (C) Higher magnification of regions 1 and 2 of Fig. 4B. Upon application of the magnetic field system, one can clearly see clusters of delivered SPION-labelled MSCs ~~within the lesion site~~ on the surface of the spinal cord (Region 1) and in the deeper area of the lesion (Region 2). Scale bar – 100 μm. (D) Overlay vector field of the calculated magnetic gradient force (*X*-*Z*-plane) with a cluster of accumulated cells. The binary image was generated from the respective fluorescent picture using ImageJ software (NIH). A representative enlarged region of the magnetic gradient force distribution (Fig. 2A) was calculated in accordance with the magnetic system positioning. The insert shows a zoomed in section of the indicated region. (E) Immunofluorescence staining of MSCs and macrophage infiltration in the lesion site. Macrophages were stained for the CD68 marker. Scale bar – 50 μm.

Figure 1.

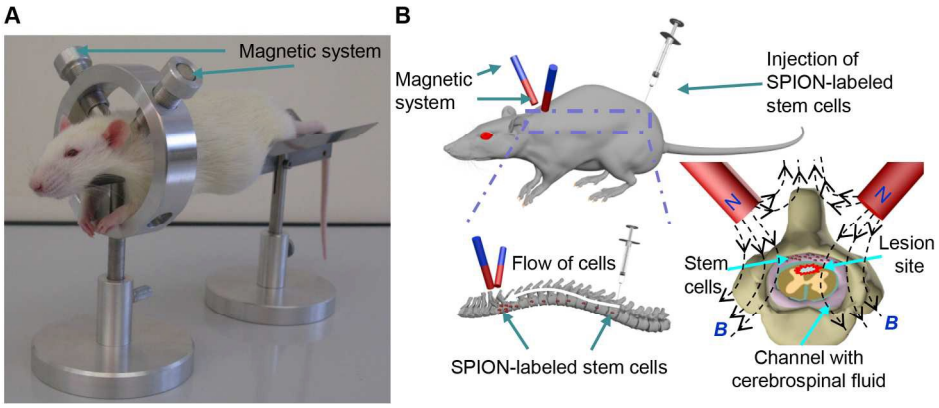

185x83mm (300 x 300 DPI)

Figure 2.

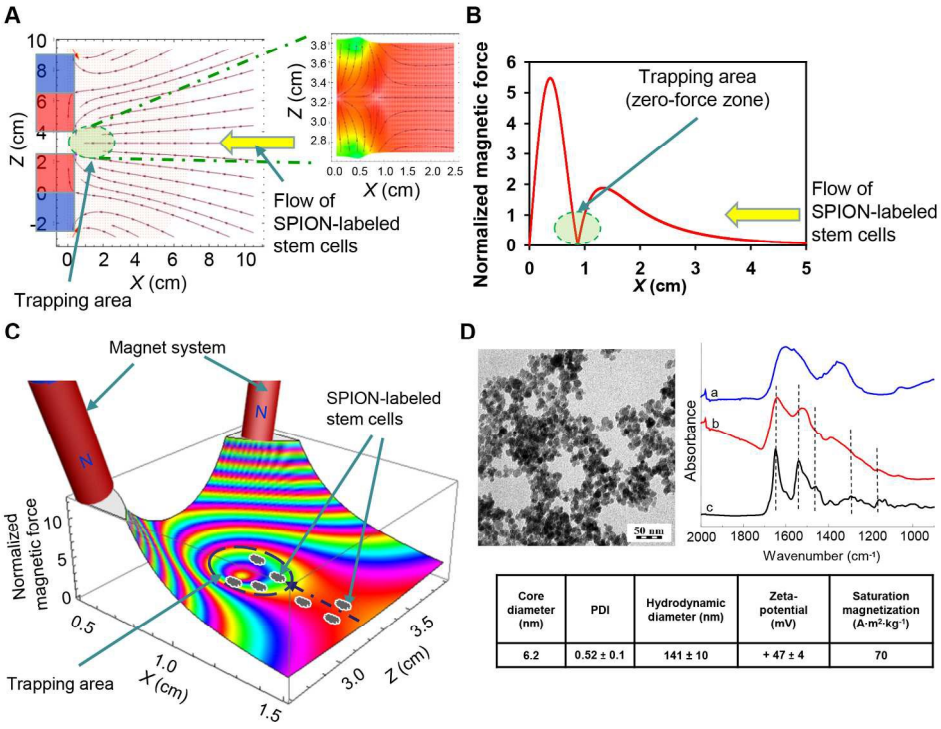

Core diameter (nm)	PDI	Hydrodynamic diameter (nm)	Zeta-potential (mV)	Saturation magnetization ($A \cdot m^2 \cdot kg^{-1}$)
6.2	0.52 ± 0.1	141 ± 10	+ 47 ± 4	70

185x141mm (300 x 300 DPI)

Figure 3.

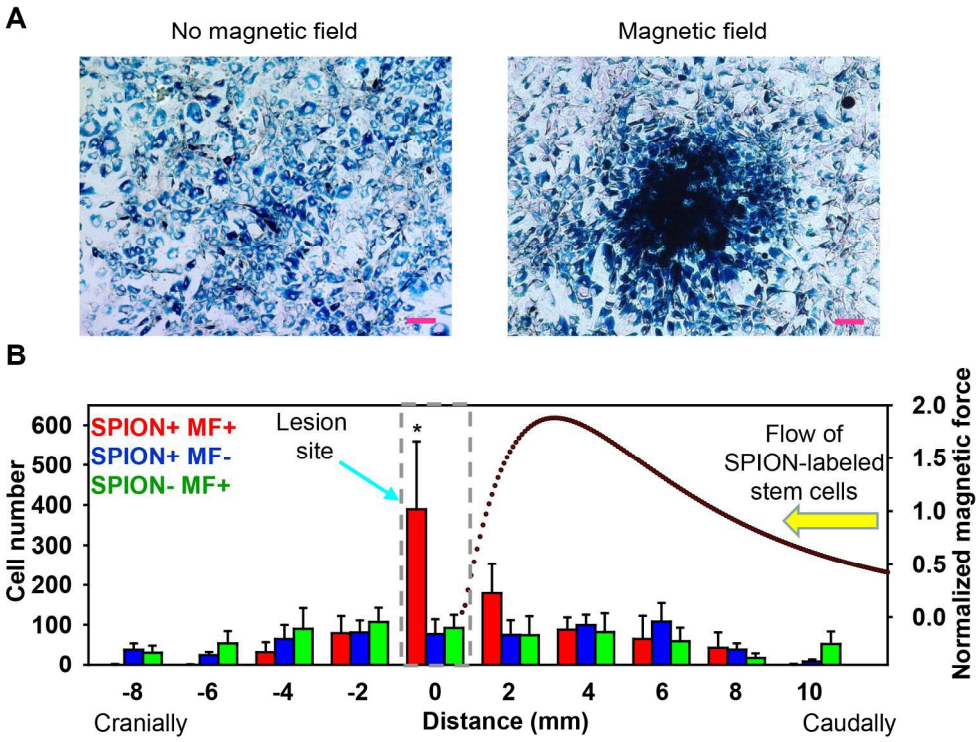

185x156mm (300 x 300 DPI)

Figure 4.

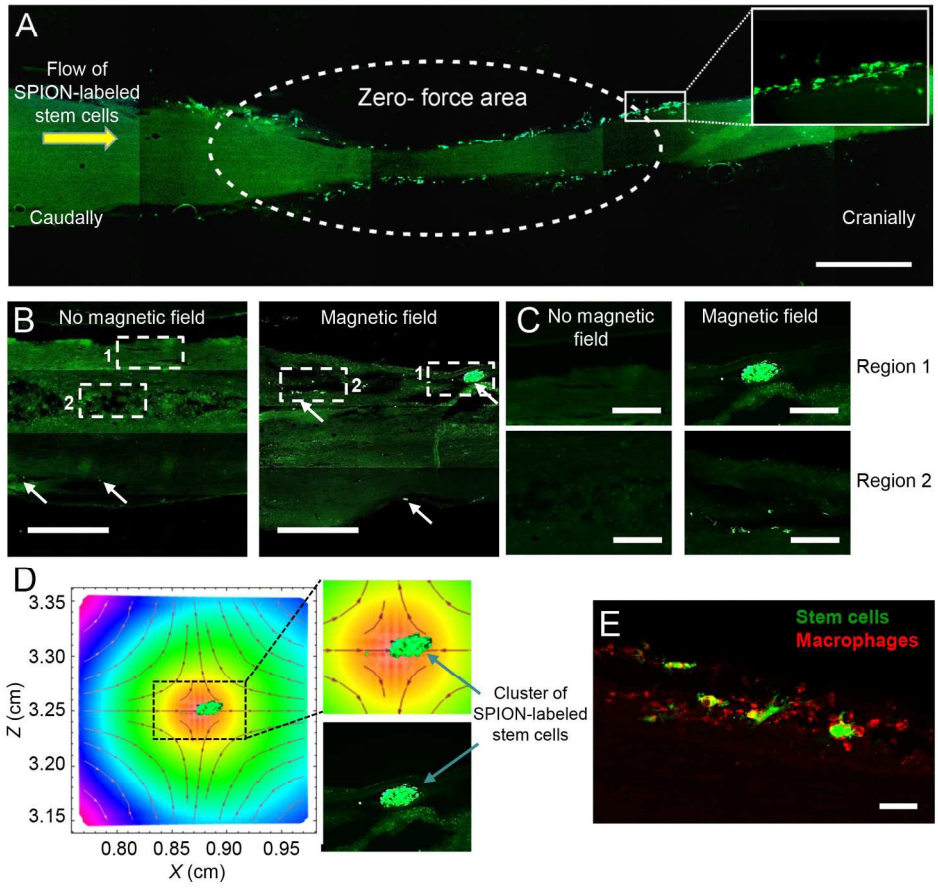

185x178mm (300 x 300 DPI)